

# Discordance of dipole asymmetries seen in recent large radio surveys with the Cosmological Principle

Ashok K. Singal<sup>\*</sup>

*Astronomy and Astrophysics Division, Physical Research Laboratory, Navrangpura, Ahmedabad - 380009, India*

Accepted XXX. Received YYY; in original form ZZZ

## ABSTRACT

In recent years, large radio surveys of Active Galactic Nuclei (AGNs), comprising millions of sources, have become available where one could investigate dipole asymmetries, assumedly arising due to a peculiar motion of the Solar system. Investigations of such dipoles have yielded in past much larger amplitudes than the cosmic microwave background (CMB) dipole, though their directions seem to lie close to the CMB dipole. Here we investigate dipole asymmetries in two recent large radio surveys, Very Large Array Sky Survey (VLASS) containing 1.9 million sources, covering the sky north of  $-40^\circ$  declination, and the Rapid ASKAP Continuum Survey (RACS) containing 2.1 million sources, covering the sky south of  $+30^\circ$  declination. We find dipoles determined from the VLASS and RACS surveys to be significantly larger than the CMB dipole. Dipole directions from the VLASS and RACS data differ significantly from each other. Nevertheless, along with a number of other previously determined dipoles, including the CMB, they all appear to lie in a narrow sky region, which argues for the various dipoles to be related somehow. However, significant differences in their derived peculiar velocities, including that of the CMB, cannot be explained by a peculiar motion of the Solar system, which should necessarily be a single value. Instead, their discordant peculiar velocities may be indicating that different cosmic reference frames are moving relative to each other or that the matter distribution on cosmic scales is not homogeneous and isotropic, either scenario being in contravention of what expected from the Cosmological Principle (CP).

**Key words:** cosmic background radiation – cosmological parameters – large-scale structure of Universe – cosmology: miscellaneous – cosmology: observations

## 1 INTRODUCTION

Peculiar motion of the Solar system can provide a direct test of the CP, according to which the various cosmic reference frames should be coincident with the reference frame defined by the CMB, with no relative motion with respect to it. However, as was first pointed out by Singal (2011), the reference frame defined by extragalactic radio sources does not seem to coincide with the CMB reference frame. Subsequent investigations have repeatedly shown that not only various cosmic reference frames seem to have relative motion with respect to the CMB reference frame, they do not seem to coincide among themselves (Rubart & Schwarz 2013; Tiwari et al. 2015; Colin et al. 2017; Bengaly, Maartens & Santos 2018; Singal 2019a,b,21,22a,b; Siewert, Rubart & Schwarz 2021; Secrest et al. 2021,22).

Due to the assumed isotropy of the Universe – à la CP – an observer stationary with respect to the comoving coordinates of the cosmic fluid, should find the distribution of distant radio sources to be uniform over the sky. However, for an observer moving with a velocity  $v$  relative to the cosmic fluid will notice, as a combined effect of aberration and Doppler

boosting, the number counts (number of sources per unit solid angle in sky) as well as the sky brightness therefrom (integrated emission from discrete sources per unit solid angle), to vary by a factor  $\propto \delta^{2+x(1+\alpha)}$ , where  $\delta = 1 + (v/c) \cos \theta$ , is the Doppler factor, assuming it to be a non-relativistic motion as shown by all previous observations (Lineweaver et al. 1996; Hinshaw et al. 2009; Singal 2011,19a,b,21,22a,b; Rubart & Schwarz 2013; Tiwari et al. 2015; Colin et al. 2017; Bengaly et al. 2018; Aghanim et al. 2020; Siewert et al. 2021; Secrest et al. 2021,22). Here  $c$  is the velocity of light,  $\alpha$  ( $\approx 0.8$ ) is the spectral index, defined by  $S \propto \nu^{-\alpha}$ , and  $x$  is the index of the integral source counts of extragalactic radio source population, which follows a power law,  $N(> S) \propto S^{-x}$  ( $x \sim 1$ ) (Ellis & Baldwin 1984; Crawford 2009; Singal 2011,14) This implies the number counts and the sky brightness will display a dipole anisotropy over the sky with an amplitude

$$\mathcal{D} = [2 + x(1 + \alpha)] \frac{v}{c}. \quad (1)$$

A dipole anisotropy in the CMB has yielded for the peculiar velocity a value  $370 \text{ km s}^{-1}$  along right ascension (RA) =  $168^\circ$ , declination (Dec) =  $-7^\circ$  or in galactic coordinates,  $l = 264^\circ$ ,  $b = 48^\circ$  (Lineweaver et al. 1996; Hinshaw et al. 2009; Aghanim et al. 2020). A couple of initial investigations declared the radio source dipoles, because of their

<sup>\*</sup> E-mail: ashokkumar.singal@gmail.com

large known as well as unknown uncertainties, to be in concordance with the CMB dipole (Baleisis et al. 1998; Blake & Wall 2002). In fact, detailed calculations showed that a positive detection of a radio dipole, at least to a minimum acceptable significant level ( $\gtrsim 3\sigma$ ), would not indeed be possible from the contemporary radio surveys, like the NRAO VLA Sky Survey (NVSS) comprising 1.8 million discrete radio sources (Condon et al. 1998), as the statistical uncertainties would match the signal indicated by the CMB dipole (Crawford 2009). It was envisaged that in order to detect a radio dipole at a statistically significant level, one might have to wait for the much larger, future radio surveys, like those planned from the Low Frequency Array (LOFAR) or the Square Kilometer Array (SKA) (Crawford 2009). However, in spite of these discouraging prognostications, a dipole was detected from the NVSS data, in the number counts as well as in the sky brightness, which first time gave a rather high value of the solar peculiar velocity,  $\sim 4$  times that expected from the CMB dipole, at a statistically significant ( $\sim 3\sigma$ ) level (Singal 2011). This positive detection became possible only because the dipole amplitude had turned out, unexpectedly, to be much larger than the CMB dipole while the statistical uncertainties, as predicted, were of the same order as the CMB dipole amplitude. Nevertheless, in spite of the large difference in amplitude, the velocity vector direction, within statistical uncertainties, turned out surprisingly coincident with the CMB dipole. With the hope that it might help resolve the issue of the difference seen in amplitudes of the NVSS and CMB dipoles, another large radio catalogue, TIFR GMRT Sky Survey (TGSS) (Swarup et al. 1991), comprising 0.62 million sources (Intema et al. 2017), was explored for any dipole asymmetries, however, it instead showed a still larger dipole anisotropy, amounting to a peculiar velocity  $\sim 10$  times the CMB value, at a very significant level ( $> 10\sigma$ ) (Bengaly et al. 2018; Singal 2019a), though even here the direction of motion turned out to be close to the CMB dipole. Similar large, though many times differing, amplitudes for various AGN dipoles, but broadly in the same direction as the CMB dipole, have since been confirmed by a number of many independent research groups (Rubart & Schwarz 2013; Tiwari et al. 2015; Colin et al. 2017; Singal 2019b, 21, 22a, b; Siewert et al. 2021; Secrest et al. 2021, 22). A significant difference between dipole amplitudes would imply a relative motion between the corresponding cosmic reference frames or inhomogeneities and anisotropies on cosmic scales, either of which will be against the CP on which the whole modern cosmology is based upon. This makes it imperative that investigations of radio dipoles, possibly, be made using many more independent datasets.

On the other hand a recent investigation (Darling 2022) of the number counts as well as the sky brightness, using a combined data from two independent catalogues, the Very Large Array Sky Survey (VLASS) (Gordon et al. 2021) and the Rapid ASKAP Continuum Survey (RACS) (Hale et al. 2021) seems to have yielded a value for the radio dipole, however, in apparent agreement with the CMB dipole, both in direction and amplitude, which contradicts almost all earlier findings for all such dipoles (Singal 2011, 19a, b, 21, 22a, b; Rubart & Schwarz 2013; Tiwari et al. 2015; Colin et al. 2017; Bengaly et al. 2018; Siewert et al. 2021; Secrest et al. 2021). As has been emphasized (Secrest et al. 2022), if the combined catalogue gives results in agreement with the CMB dipole,

individual catalogues, which are sufficiently large, too should yield similar results. Because the question involved here is of rather crucial relevance for cosmological studies, where at stake is the CP itself, we investigate here the radio dipoles in each of the VLASS as well as RACS samples, individually, and in sufficient details.

## 2 VLASS AND RACS DATASETS

The Very Large Array Sky Survey (VLASS) at 3 GHz (Lacy et al. 2020), carried out at Karl G. Jansky Very Large Array, covering the sky north of  $-40^\circ$  declination, contains 1.9 million sources (Gordon et al. 2021). Another version of the above catalogue from an independent reduction of the survey data is also available (Bruzewski et al. 2021), which, in order to distinguish, we call here VLASS-B. The Rapid ASKAP Continuum Survey (RACS), covering the sky south of  $+30^\circ$  declination at 887.5 MHz, carried out using the Australian Square Kilometre Array Pathfinder (ASKAP) contains 2.1 million sources (Hale et al. 2021).

In our investigations, we are looking for a dipole in distribution of source positions in the sky where any gaps in the sky coverage can affect the dipole estimates. However, exclusion of sky-strips, which affect the forward and backward measurements identically, for example symmetric strips in diametrically opposite regions on the sky, to a first order do not have systematic effects on the inferred direction of the dipole (Ellis & Baldwin 1984), apart from the errors becoming larger because of lesser data. Since the VLASS catalogue (Gordon et al. 2021) has a gap of sources for  $\text{Dec} < -40^\circ$ , we drop all sources with  $\text{Dec} > 40^\circ$  as well to have equal and opposite gaps on two opposite sides. We also exclude all sources from our sample which lie in the Galactic plane ( $|b| < 10^\circ$ ). Similarly from the RACS catalogue (Hale et al. 2021), we dropped all sources with  $\text{Dec} < -30^\circ$  as well as  $|b| < 10^\circ$ .

The integrated source counts,  $N(> S)$  for different  $S$  for the VLASS and RACS samples are shown in Fig. 1. The index  $x$  in the power law relation,  $N(> S) \propto S^{-x}$ , estimated from the slope of the  $\log N - \log S$  plot in Fig. 1, can be seen to steepen from low to high flux-density levels for both samples. From piece-wise straight line fits to the  $\log N - \log S$  data, we find that  $x$  steepens from 0.9 to 1.15 around 10 mJy in the VLASS data, while in the RACS sample it steepens from 0.75 to 0.9 around 15-20 mJy. These breaks in the index values seem to indicate intrinsic changes in the source count indices. We restrict our investigations to flux densities 10 mJy or above for the VLASS data and to flux densities 20 mJy or above for the RACS data and use the corresponding values of  $x = 1.15$  for the VLASS sample and  $x = 0.9$  for the VLASS sample in Eq. (1), while deriving the peculiar velocities from the observed values of dipole amplitude,  $\mathcal{D}$ , in each case. As earlier measurements have shown the peculiar velocity estimates to be about 2 to 20 times higher than the CMB value of  $370 \text{ km s}^{-1}$ , for convenience of comparison we use a parameter  $p$  for the amplitude of the peculiar velocity  $v$ , in units of the CMB value  $370 \text{ km s}^{-1}$ , so that  $v = p \times 370 \text{ km s}^{-1}$ , with  $p = 0$  implying a nil peculiar velocity while  $p = 1$  implying the CMB value.

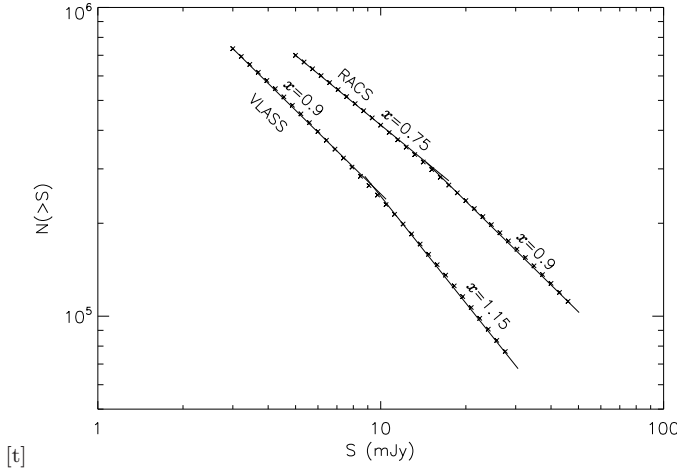


**Figure 1.** A plot of the integrated source counts  $N(>S)$  against  $S$ , for the VLASS and RACS samples, showing the power law behavior ( $N(>S) \propto S^{-x}$ ) of the source counts. From piece-wise straight line fits to data in different flux-density ranges in either sample, index  $x$  appears to steepen for stronger sources, as shown by continuous lines with the best-fit index values written above.

### 3 METHOD AND PROCEDURE

#### 3.1 Dipole vector determined from a sum of position vectors of the sources

We can determine the solar peculiar velocity from a dipole in the distribution of source positions in sky. The direction of the dipole is first determined from the vector sum,  $\sum_{i=1}^N \hat{\mathbf{r}}_i$ , where  $\hat{\mathbf{r}}_i$  is the angular position vector of  $i$ th source in sky and  $N$  is the total number of sources in the sample used (Crawford 2009; Singal 2011). Then with  $\hat{\mathbf{d}}$  as a unit vector in the direction of the dipole, amplitude of the dipole is computed from

$$\mathcal{D} = \frac{3 \sum_{i=1}^N \hat{\mathbf{d}} \cdot \hat{\mathbf{r}}_i}{2 \sum_{i=1}^N |\hat{\mathbf{d}} \cdot \hat{\mathbf{r}}_i|} = \frac{3}{2} \frac{\sum_{i=1}^N \cos \theta_i}{\sum_{i=1}^N |\cos \theta_i|}, \quad (2)$$

where  $\theta_i$  is the polar angle of the  $i$ th source with respect to the determined dipole direction. The statistical uncertainty in estimated  $\mathcal{D}$  is  $\sqrt{3/N}$  (Crawford 2009; Singal 2011).

If in place of  $\cos \theta_i$  one uses  $S_i \cos \theta_i$  within summations in both numerator and denominator in Eq. (2), where  $S_i$  is the observed flux density of the  $i$ th source, then one begets dipole  $\mathcal{D}$  from the sky brightness due to radio sources. Of course Eq. (1) still gives the peculiar velocity from  $\mathcal{D}$  thus computed. However, in Eq. (6) of Darling(2022), following Rubart & Schwarz (2013), an extra factor of  $\delta^{1+\alpha}$  due to Doppler boosting in the integrated flux density per solid angle was included, which is erroneous. Actually in an *observed* flux-density range, which is chosen to be the same for all directions in sky, one multiplies  $S$  with the number of sources visible to the observing instrument at that flux density level. For instance, the contribution to the sky brightness at an observed flux density  $S$  comes from sources whose rest-frame flux density is  $S/\delta^{1+\alpha}$ . Thus the flux boosting of individual sources, pointed out in Darling(2022) for the formula already gets compensated for because of the fact that in the rest frame the sources were intrinsically weaker by a factor  $\delta^{(1+\alpha)}$ . Of course, as a result, the number of sources at the flux den-

sity  $S$  alter by a factor  $\delta^{x(1+\alpha)}$ , while the Doppler boosting by the factor  $\delta^{1+\alpha}$  is already accounted for in the altered number of sources in that observed flux-density bin for every direction in sky. All this has been pointed out and discussed in detail already (Singal 2014), where it was shown that the correct formula to compute the peculiar velocity from the sky brightness is the same as in Eq. (1) here, and which has been employed earlier for this purpose (Singal 2011).

Further, in the sky brightness method, a relatively small number of strong sources at high flux-density levels could introduce large statistical fluctuations (Singal 2011), therefore one ends up putting an upper limit on the flux density of sources in the sample to be employed. However, in the the number counts (Eq. (2)), unlike in the case of sky brightness, a small number of bright sources do not adversely affect the results, therefore, we have chosen to restrict our analysis here to number counts only.

#### 3.2 Hemisphere method with respect to the estimated dipole direction

Dipole magnitude can be estimated in another way called hemisphere method, which, unlike the vector method described in section 3.1, does not directly yield the direction of the dipole. Since we do not know the dipole direction, we have to start with a certain assumed direction for the dipole and compute the magnitude of the dipole in that direction. It could, for example, be taken from the already known direction, like that of the CMB, or it be taken from the direction  $\hat{\mathbf{d}}$  of the dipole as determined from the vector method. Then the sky is divided in two hemispheres,  $H1$  and  $H2$ , with  $H1$  centred on the assumed direction of the dipole and  $H2$  centred on the opposite direction. If  $N_1$  is the number of sources found in  $H1$  and  $N_2$  is that found in  $H2$ , then the dipole  $\mathcal{D}$  could be determined from the observed fractional excess of  $N_1$  over  $N_2$  as

$$\mathcal{D} = 2 \frac{\delta N}{N} = 2 \frac{N_1 - N_2}{N_1 + N_2}. \quad (3)$$

while the error in  $\mathcal{D}$  in the hemisphere method is  $2/\sqrt{N}$  (Singal 2019a).

However, we may not want to get biased by an already known direction like that from the CMB, and might like to determine the direction of the dipole independent of the vector method as well. In that case, we can employ a ‘brute force’ method (Singal 2019b). We divide the sky into small pixels of angular area, say  $\Delta\theta \times \Delta\theta$ , creating a grid of  $n$  cells covering the whole sky area of  $4\pi$  sr, with minimal overlaps. Then one by one, taking the trial pole direction to be the centre of each of these  $n$  pixels, and accordingly counting sources in our sample in the two hemispheres with respect to that trial pole direction, we compute the dipole amplitudes ( $p$ ), using Eqs. (1) and (3). Thus for each one of these  $n$  pixels, we have RA, Dec, and a peculiar velocity value  $p$ . However, this  $p$  value may only be a projection of the true peculiar velocity along the corresponding RA and Dec. Therefore, we can expect a peak along the real dipole direction, along with a  $\cos \psi$  dependence in the  $p$  values, determined for the other  $n-1$  grid points around it.

The location of the peak value for the dipole amplitude, in principle, should yield the true direction of the dipole. However, because of statistical fluctuations in individual values,

**Table 1.**Peculiar velocity vector from number counts for the VLASS dataset with  $|\delta| < 40^\circ$ 

(1) Flux-density (mJy)	(2) $N$	(3) RA ( $^\circ$ )	(4) Dec ( $^\circ$ )	(5) $\mathcal{D}$ ( $10^{-2}$ )	(6) $p$ ( $370 \text{ km s}^{-1}$ )	(7) $\mathcal{D}_h$ ( $10^{-2}$ )	(8) $p_h$ ( $370 \text{ km s}^{-1}$ )
$\geq 50$	36532	$160 \pm 21$	$00 \pm 27$	$2.2 \pm 1.0$	$4.4 \pm 2.0$	$1.9 \pm 1.0$	$3.8 \pm 2.1$
$\geq 30$	69465	$174 \pm 15$	$13 \pm 25$	$1.9 \pm 0.7$	$3.8 \pm 1.4$	$2.2 \pm 0.8$	$4.4 \pm 1.5$
$\geq 20$	112322	$188 \pm 14$	$28 \pm 23$	$1.8 \pm 0.6$	$3.5 \pm 1.1$	$2.5 \pm 0.6$	$5.0 \pm 1.2$
$\geq 10$	240458	$189 \pm 12$	$42 \pm 22$	$1.9 \pm 0.4$	$3.8 \pm 0.8$	$2.1 \pm 0.4$	$4.3 \pm 0.8$

**Table 2.**Peculiar velocity vector from number counts for the VLASS-B dataset with  $|\delta| < 40^\circ$ 

(1) Flux-density (mJy)	(2) $N$	(3) RA ( $^\circ$ )	(4) Dec ( $^\circ$ )	(5) $\mathcal{D}$ ( $10^{-2}$ )	(6) $p$ ( $370 \text{ km s}^{-1}$ )	(7) $\mathcal{D}_h$ ( $10^{-2}$ )	(8) $p_h$ ( $370 \text{ km s}^{-1}$ )
$\geq 50$	35447	$182 \pm 20$	$01 \pm 27$	$1.1 \pm 1.0$	$2.3 \pm 2.0$	$1.7 \pm 1.1$	$3.4 \pm 2.1$
$\geq 30$	68833	$176 \pm 16$	$22 \pm 25$	$1.3 \pm 0.7$	$2.5 \pm 1.4$	$1.9 \pm 0.8$	$3.8 \pm 1.5$
$\geq 20$	112017	$192 \pm 15$	$46 \pm 24$	$1.6 \pm 0.6$	$3.1 \pm 1.2$	$1.9 \pm 0.6$	$3.9 \pm 1.2$
$\geq 10$	237456	$215 \pm 15$	$52 \pm 23$	$2.1 \pm 0.4$	$4.1 \pm 0.8$	$2.2 \pm 0.4$	$4.5 \pm 0.8$

it may not always be possible to zero down on a single unique peak for the true dipole direction. Nevertheless, we can refine the procedure for determining the pole direction by making use of the expected  $\cos \psi$  dependence of  $p$  for grid points at polar angle  $\psi$  from the true pole.

We have written a COSFIT routine which, for each one of the  $n$  sky positions, makes 3-d cos fits to the  $p$  values of surrounding  $n - 1$  pixels around it, and determines the sky position of the pixel that yields the highest value, which then would be the optimum direction for the peculiar motion. One could also evaluate the  $\chi^2$  value from the residuals to each of these  $n$  3-d cos fits to the expected  $\cos \psi$  dependence, its minimum should also occur close to the true direction of the peculiar motion.

## 4 RESULTS AND DISCUSSION

The results for the dipole, determined using the vector method (section 3.1) from the anisotropy in number counts in the VLASS sub-samples at four different flux-density levels, are presented in Table 1, where column (1) gives the flux-density limit of the sub-sample, column (2) gives the number of sources in the sub-sample, columns (3) and (4) list the direction of the dipole in terms of right ascension and declination, derived from the vector dipole method applied to that sub-sample, column (5) gives  $\mathcal{D}$ , the dipole magnitude computed from Eq. (2), and column (6) lists  $p$ , the peculiar speed estimated from  $\mathcal{D}$  using Eq. (1). Columns (7) and (8) list dipole  $\mathcal{D}_h$ , and peculiar speed,  $p_h$ , determined from the hemisphere method (section 3.2), for the direction given in columns (3) and (4) for the corresponding sub-sample. From Table 1 we find the peculiar speed from the VLASS data in various flux-density bins to be about four times the peculiar speed estimated from the CMB dipole. The peculiar velocity  $v$  can be calculated from  $p$  as  $v = p \times 370 \text{ km s}^{-1}$ .

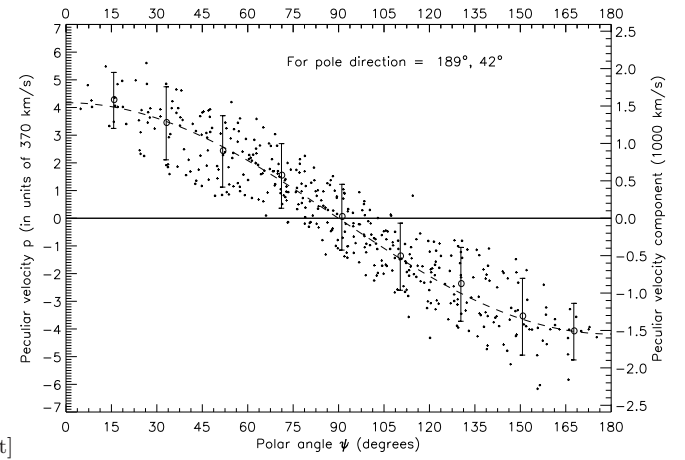
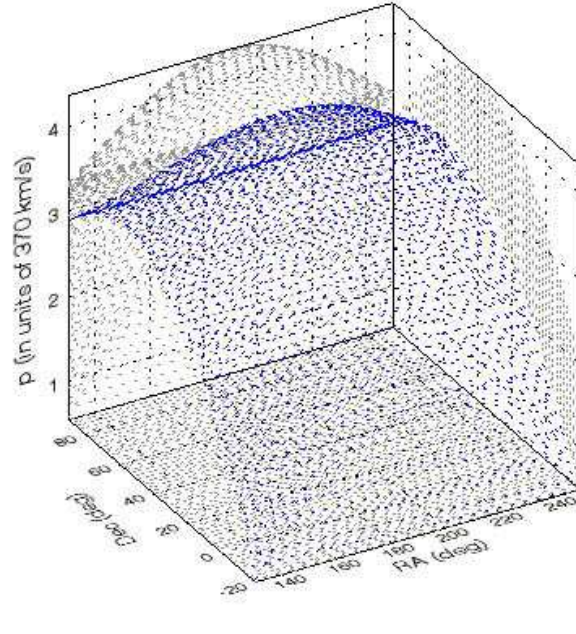


**Figure 2.** Variation of the peculiar velocity component  $p$  (in units of CMB value  $370 \text{ km s}^{-1}$ ), computed for various polar angles with respect to the dipole direction, RA =  $189^\circ$ , Dec =  $42^\circ$ , derived by the dipole vector method for the  $S \geq 10 \text{ mJy}$  sub-sample (Table 1). The corresponding peculiar velocity values of the solar system in units of  $10^3 \text{ km s}^{-1}$  are shown on the right hand vertical scale. Plotted circles (o) with error bars show values for bin averages of the peculiar velocity components, obtained for various  $20^\circ$  wide slices of the sky in polar angle, while the dashed line shows a least square fit of  $\cos \psi$  to the bin average values.

From Table 1 we see a trend that the direction of the dipole from VLASS data seems to shift northward with lower flux-density levels. In fact the direction of the dipole at  $\geq 30 \text{ mJy}$  levels might appear to be in agreement with the CMB dipole (RA =  $168^\circ$ , Dec =  $-7^\circ$ ), but as we go to the lower flux-density levels ( $\geq 10 \text{ mJy}$ ) the direction of the determined dipole shifts significantly away from the CMB dipole, especially in declination.



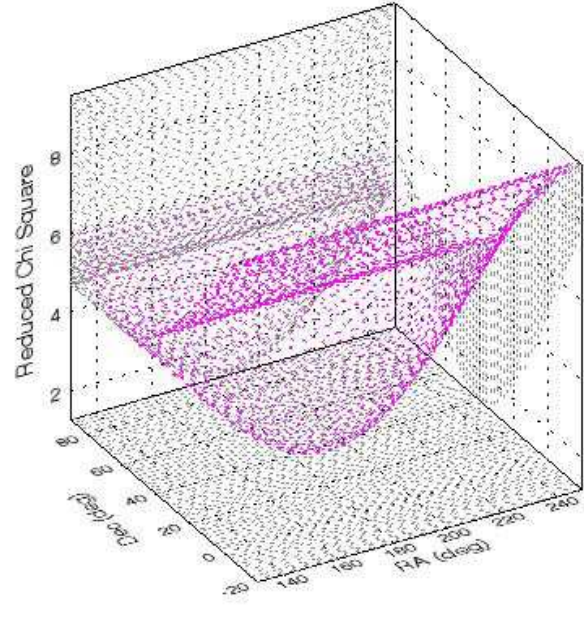
[t]

**Figure 3.** A plot of 3-d cos fits made to the dipole amplitudes estimated for various trial dipole directions across the sky, showing a unique unambiguous peak indicating the optimum direction of the dipole. The horizontal axes denote right ascension (RA) and declination (Dec) in degrees. The positions (RA and Dec) of the extrema are determined more easily from the 2-d projections, shown in light gray, thence we infer the direction of the observer’s peculiar velocity as RA = 189°, and Dec = 42°.

In order to ascertain whether this trend is genuinely present in the VLASS data, we have also determined the dipoles in the VLASS-B data (Bruzewski et al. 2021) and the results are presented in Table 2. Although entries in Table 1 and Table 2 may seem to differ in details, the overall results appear to be in agreement. A similar trend of a shift in the dipole position in declination with decreasing flux levels is seen in both Table 1 and Table 2.

To determine the dipole direction in sky from the hemisphere method (section 3.2) using the brute force technique (Singal 2019b), we first divided the sky into  $10^\circ \times 10^\circ$  pixels with minimal overlap, thereby creating a grid of 422 cells covering the whole sky. Then taking the dipole direction to be the centre of each of these 422 cells, in turn, counted the number of sources in corresponding hemispheres  $H1$  and  $H2$  for a sample chosen from say,  $S \geq 10$  mJy (Table 1), and using Eq. (3) computed the dipole magnitude  $p_i$  for  $i = 1$  to 422. Actually this yields only a projection of the peculiar velocity in the direction of  $i$ th pixel, which should have a  $\cos \psi_i$  dependence where  $\psi_i$  is a polar angle of  $i$ th pixel with respect to the actual pole.

In order to test this  $\cos \psi$  dependence, we have plotted in Fig. (2) the peculiar velocity components  $p_i$  for various  $n$  points, as a scatter plot for different  $\psi_i$  values, measured with respect to the direction, RA = 189°, Dec = 42°, derived from dipole vector method, (Table 1,  $S \geq 10$  mJy). We also computed bin averages of peculiar velocity  $p$  in  $20^\circ$  wide slices of the sky by divided the sky into bins of  $20^\circ$  width in polar angle about the above pole position, viz. RA = 189°, Dec = 42°.



[t]

**Figure 4.** Reduced Chi-squared ( $\chi^2_\nu$ ) values for the 3-d cos fits, made to the dipole amplitudes estimated for various trial dipole directions across the sky, shows a minimum value of 1.2, quite close to the ideal minimum value of unity, at exactly the same sky position, RA = 189°, and Dec = 42°, as the peak in Fig. (3).

A least square fit of  $\cos \psi$  to the bin average values (Fig. (2)) shows that the computed  $p$  values for various pixels at polar angles ( $\psi$ ) do follow a systematic  $\cos \psi$  dependence.

We now made a 3-d  $\cos \psi$  fit for each of the  $n = 422$  positions for the remaining  $n - 1$   $p$  values, and also computed the chi-square value for each of these  $n$  fits. This COSFIT routine resulted in a clear unique peak, indicating the optimum direction of the dipole (Fig. (3)). A reduced Chi-squared ( $\chi^2_\nu$ ) values for the 3-d cos fits made to the dipole amplitudes estimated for various trial dipole directions across the sky, shows a minimum value of 1.2 (Fig. (4)), quite close to the ideal minimum value of unity (Bevington & Robinson 2003), at the same sky position as the peak in (Fig. (3)). Thence we infer the direction of the observer’s peculiar velocity as RA = 189°, and Dec = 42°, which agrees very well with the corresponding value (RA = 189°, Dec = 42°), derived directly from the dipole vector method (Table 1,  $S_{3\text{GHz}} \geq 10$  mJy). We also tried finer grids with  $5^\circ \times 5^\circ$  bins with 1668 cells and even a grid with  $2^\circ \times 2^\circ$  bins with 10360 cells, but it made no perceptible difference in the results.

The dipole amplitude distribution across the sky is shown in a contour map for the VLASS data for the  $S \geq 10$  mJy sub-sample (Fig. 5). A broad plateau showing maxima in  $p$ , towards certain sky directions is clearly seen, however, from that it is not possible to zero down on a single unique peak for the true dipole direction. Therefore we used our COSFIT routine to minimize  $\chi^2$  to determine the optimum direction for the VLASS dipole, which is indicated in Fig. 5 by the symbol  $\oplus$ . The symbol  $\odot$  indicates the CMB pole position on the map.

The results for the dipole, determined from the anisotropy in number counts in the RACS sample at four different flux-

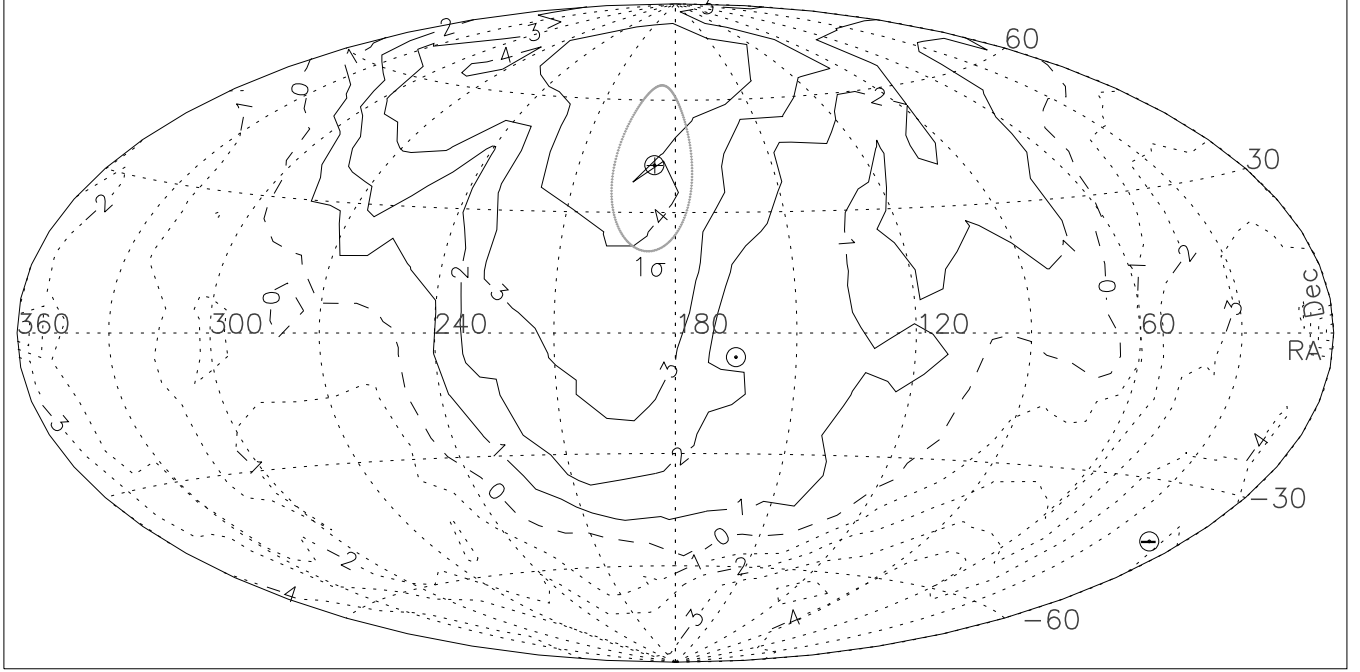


**Figure 5.** A contour map of the dipole amplitudes, in the Hammer–Aitoff equal-area projection on the sky, estimated for various directions in the sky, from the VLASS data. The horizontal and vertical axes denote RA, from  $0^\circ$  to  $360^\circ$ , and Dec from  $-90^\circ$  to  $90^\circ$ . The true pole direction is expected to be closer to the higher contours values, shown by continuous lines, while the true antipole should lie closer to the lower contour values, shown by dotted lines. The dashed curve represents the zero amplitude of the dipole. The symbol  $\oplus$  indicates the best-fit pole position for the VLASS sample, derived using our COSFIT routine to minimize  $\chi^2$  (see the text), while the symbol  $\ominus$  indicates the corresponding antipole position. The gray-color error ellipse around the best-fit position  $\oplus$  represents the  $1\sigma$  (68.3%) confidence limits. The symbol  $\odot$  indicates the CMB pole position.

**Table 3.**

Peculiar velocity vector from number counts for the RACS dataset with  $|\delta| < 30^\circ$  and  $|b| > 10^\circ$

(1) Flux-density (mJy)	(2) $N$	(3) RA ( $^\circ$ )	(4) Dec ( $^\circ$ )	(5) $\mathcal{D}$ ( $10^{-2}$ )	(6) $p$ ( $370 \text{ km s}^{-1}$ )	(7) $\mathcal{D}_h$ ( $10^{-2}$ )	(8) $p_h$ ( $370 \text{ km s}^{-1}$ )
$\geq 100$	49711	$200 \pm 25$	$-39 \pm 31$	$4.6 \pm 0.9$	$10.2 \pm 2.0$	$4.5 \pm 0.9$	$10.0 \pm 2.0$
$\geq 50$	102837	$193 \pm 17$	$-41 \pm 30$	$3.9 \pm 0.6$	$8.7 \pm 1.4$	$3.7 \pm 0.6$	$8.2 \pm 1.4$
$\geq 30$	166423	$197 \pm 14$	$-42 \pm 28$	$3.9 \pm 0.5$	$8.7 \pm 1.1$	$3.3 \pm 0.5$	$7.3 \pm 1.1$
$\geq 20$	236887	$197 \pm 13$	$-43 \pm 23$	$4.0 \pm 0.4$	$8.9 \pm 0.9$	$3.3 \pm 0.4$	$7.3 \pm 0.9$

density levels, are presented in Table 3, where we see that the direction of the dipole is almost independent of the chosen flux-density levels, but is significantly away from the CMB dipole ( $\text{RA} = 168^\circ$ ,  $\text{Dec} = -7^\circ$ ). The dipole amplitude distribution across the sky for the RACS data is shown in a contour map for the  $S \geq 20 \text{ mJy}$  sub-sample (Fig. 6). Again, a broad plateau showing maxima in  $p$ , towards certain sky directions is clearly seen, however, from that it is not possible to zero down on a single unique peak for the true dipole direction. Therefore we used our COSFIT routine to find the optimum direction for the peculiar motion, which is indicated in Fig. 6 by the symbol  $\oplus$ . The symbol  $\odot$  indicates the CMB pole position on the map.

A major effort was put into testing the procedure and estimation of uncertainties, especially in the sky position estimates of the dipoles. For that we used Monte–Carlo simulations to create an artificial radio sky with similar number

densities of sources as in each of the two catalogues, by randomly assigning sky positions, for the observed flux-density values in each sub-sample, so that overall source counts remain unchanged. On these we superimposed Doppler boosting and aberration effects of an assumed solar peculiar motion, choosing in each simulation a different direction in sky for the assumed velocity vector. This mock catalogue was then used to retrieve the velocity vector under the conditions of zone of avoidance in the galactic plane ( $|b| < 10^\circ$ ) or declination restrictions ( $|\delta| < 40^\circ$  or  $|\delta| < 30^\circ$ , as the case may be) similar as in our actual VLASS or RACS samples and compared with the input velocity vector in that particular realization. This not only validated our procedure as well as the computer routine, but also helped us make an estimate of errors in the dipole co-ordinates from 500 simulations we made in either case, using a different mock dipole vector in sky for each simulation.

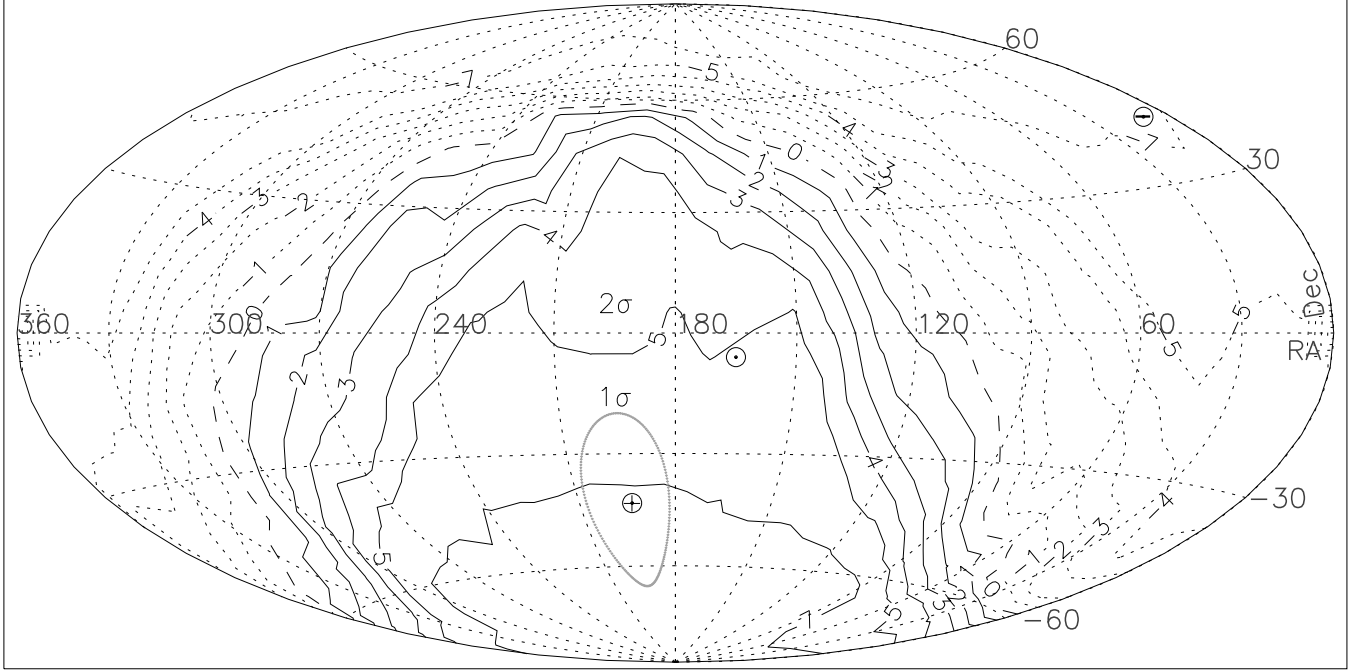


**Figure 6.** A contour map of the dipole amplitudes for the RACS data, estimated for various directions in the sky. The horizontal and vertical axes denote RA and Dec in degrees. The true pole direction is expected to be closer to the higher contours values, shown by continuous lines, while the true antipole should lie closer to the lower contour values, shown by dotted lines. The dashed curve represents the zero amplitude of the dipole. The symbol  $\oplus$  indicates the best-fit pole position for the RACS sample, derived using our COSFIT routine to minimize  $\chi^2$ , while the symbol  $\ominus$  indicates the corresponding antipole position. The gray-color error ellipse around the best-fit position  $\oplus$  represents the  $1\sigma$  (68.3%) confidence limits. The symbol  $\odot$  indicates the CMB pole position.

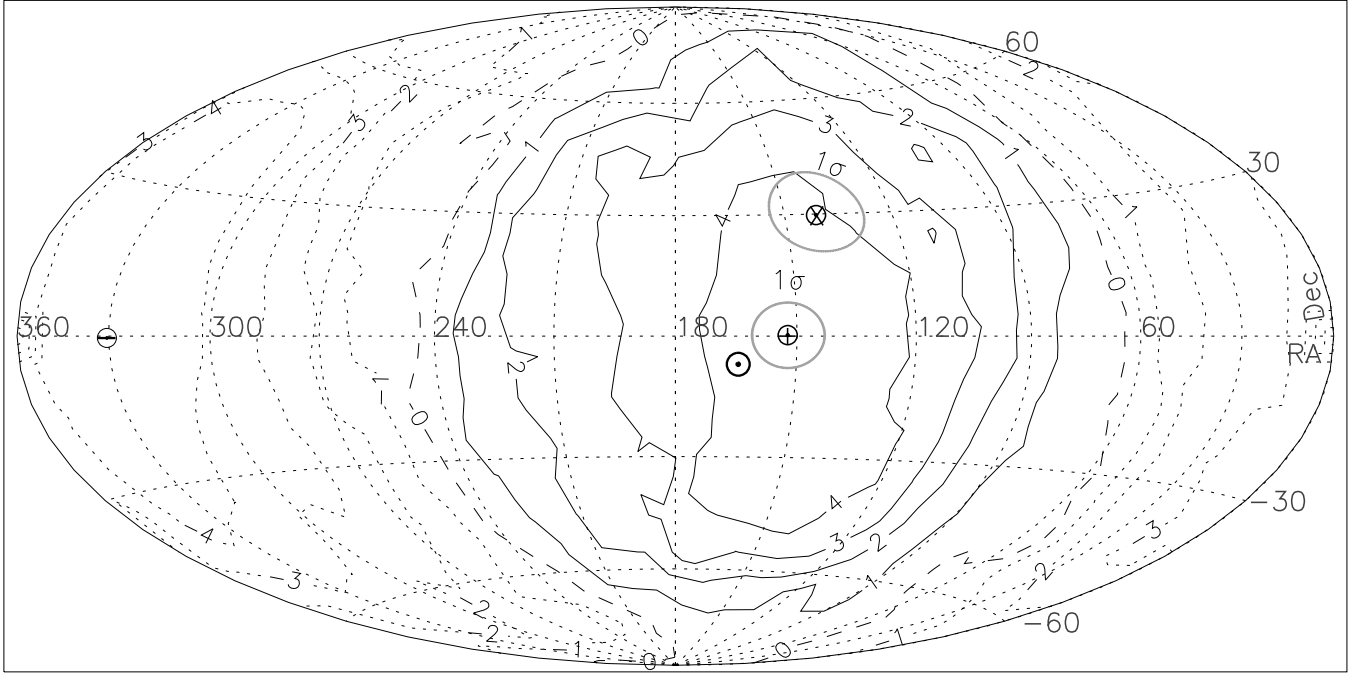


**Figure 7.** A contour map of the dipole amplitudes for the NVSS data, estimated for various directions in the sky. The horizontal and vertical axes denote RA and Dec in degrees. The true pole direction is expected to be closer to the higher contours values, shown by continuous lines, while the true antipole should lie closer to the lower contour values, shown by dotted lines. The dashed curve represents the zero amplitude of the dipole. The symbol  $\oplus$  indicates the best-fit pole position for the NVSS sample, derived using our COSFIT routine to minimize  $\chi^2$ , while the symbol  $\ominus$  indicates the corresponding antipole position. The symbol  $\otimes$  indicates another estimate of the dipole position, derived from an alternate method (see text). The gray-color error ellipses around  $\oplus$  and  $\otimes$  represent the  $1\sigma$  (68.3%) confidence limits about the corresponding pole positions.

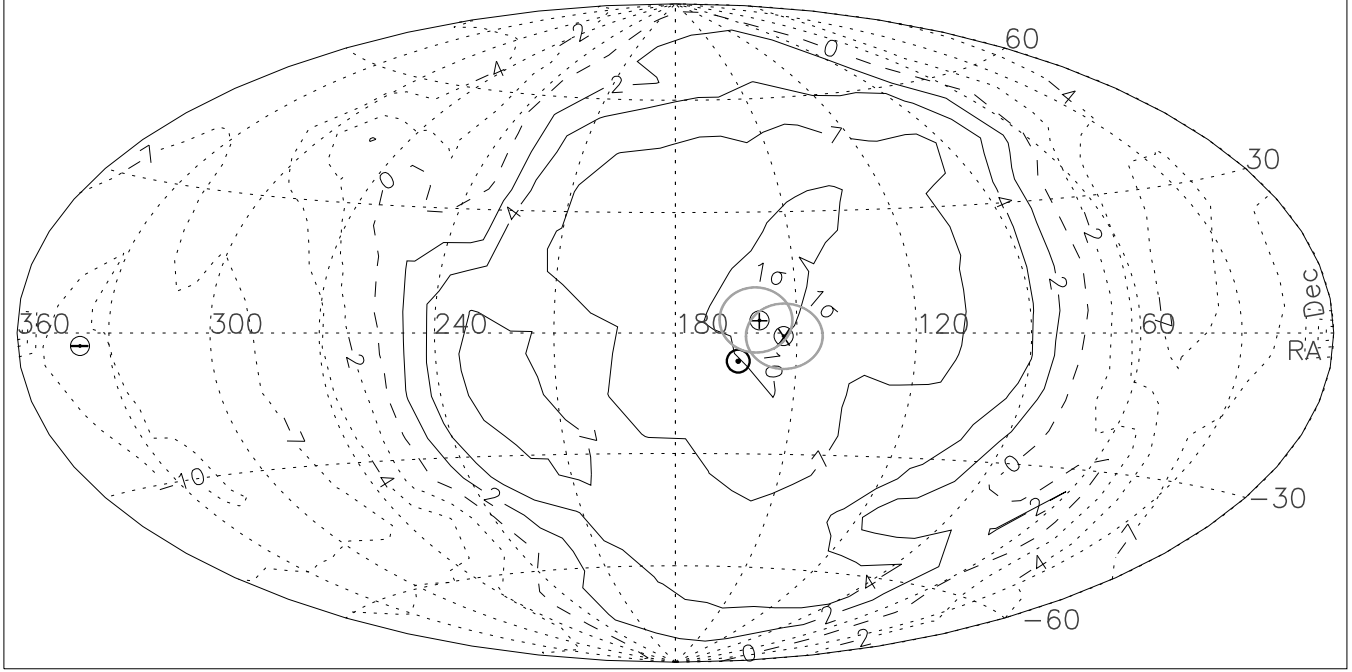


**Figure 8.** A contour map of the dipole amplitudes for the TGSS data, estimated for various directions in the sky. The horizontal and vertical axes denote RA and Dec in degrees. The true pole direction is expected to be closer to the higher contours values, shown by continuous lines, while the true antipole should lie closer to the lower contour values, shown by dotted lines. The dashed curve represents the zero amplitude of the dipole. The symbol  $\oplus$  indicates the best-fit pole position for the TGSS sample, derived using our COSFIT routine to minimize  $\chi^2$ , while the symbol  $\ominus$  indicates the corresponding antipole position. The symbol  $\otimes$  indicates another estimate of the dipole position, derived from an alternate method (see text). The gray-color error ellipses around  $\oplus$  and  $\otimes$  represent the  $1\sigma$  (68.3%) confidence limits about the corresponding pole position. The symbol  $\odot$  indicates the CMB pole position.

If we now compare the dipole determined from number counts for the VLASS dataset (Table 1 and Fig. 5) with that determined from the RACS dataset (Table 3 and Fig. 6), we find that not only the amplitudes of the dipoles but also the directions of the dipoles from both these datasets differ significantly from each other as well as from the CMB dipole. Assuming there are no declination-dependent calibration systematics in either survey, a statistically significant difference in the estimates of the two dipoles is puzzling. It is further intriguing that RACS data yields the pole positions almost independent of the flux-density levels, but VLASS data there seems to be a systematic shift to higher declinations with a decreasing flux-density level.

A combined set of data from the VLASS and RACS catalogues seems to have yielded a value for the radio dipole in apparent agreement with the CMB dipole, both in direction and amplitude (Darling 2022). Actually, in the case of VLASS and RACS, individual dipoles (Fig. 5 and 6) seem to be lying in the northern and southern hemispheres, almost equally away from the celestial equator. When combined, the asymmetric distributions of number density of sources in opposite hemispheres in the VLASS and RACS samples partly cancel these asymmetries and the inferred dipole of the combined data gives a much reduced value for the dipole amplitude and the direction somewhere in the middle of the two individual dipoles, which happens in this case to be close to the CMB dipole, and such apparently has been verified (Secrest et al. 2022). As has been emphasized earlier (Singal 2022a; Secrest et al. 2022), in combining data from two independent

catalogues to determine a dipole from number count asymmetries, there is always a possibility of getting results which might not truly represent an actual dipole in sky. In fact, a combination of two catalogues, even without any genuine dipoles or asymmetries present in their number densities, but having slightly different source number densities and covering partly different regions of sky, could yield an artificial dipole vector. The source number densities could be different due to slight mismatch in calibrations or the catalogues could be at different frequency bands and a slight uncertainty in spectral information might result in slightly different number densities of sources. After all inference of a dipole like the CMB dipole needs *overall* number densities to differ only by one part in  $10^3$  in the two separate catalogues. Thus such catalogues when combined could result in an artificial dipole because of such different number densities in two different coverage directions of the two catalogues. On the other hand, in such a combination of catalogues there might even be a cancellation of individual dipoles, which may otherwise be actually present in the two separate catalogues, as seems to be the case in VLASS and RACS catalogues.

Two other large radio surveys, NVSS and TGSS, where dipoles have been determined in past (Singal 2011; Bengaly et al. 2018; Singal 2019a), have yielded dipoles with similar larger amplitudes (by a factor of 4 to 10) than the CMB, though directions derived using dipole vector method were found to be consistent with the CMB dipole. Here we take a fresh look at the NVSS and TGSS dipoles by determining their directions using the brute force method, by minimizing

$\chi^2$  in the 3-d  $\cos\psi$  fitting using our COSFIT routine. We show in Fig. 7 a contour map of dipole components in different sky directions, determined for the NVSS sample with  $S \geq 20$  mJy (Singal 2011). The best-fit pole position for the NVSS, derived from a minimum of the reduced Chi-squared value ( $\chi^2_\nu \lesssim 1$ ), employing our COSFIT routine, is within  $\sim 1.5\sigma$  of the CMB pole position and lies inside a contour corresponding to a peculiar velocity  $p \sim 4$ . Also indicated in Fig. 7 is another estimate of the NVSS dipole position, derived from an alternate method (Secrest et al. 2022), which also lies within the highest contour in Fig. 7, however, the reduced Chi-squared values from the 3-d  $\cos\psi$  fits, made to the dipole amplitudes estimated around this particular direction, shows  $\chi^2_\nu \approx 3.0$ , much above the minimum value. It should be noted that the direction for our best-fit pole position comes not from the dipole amplitude values on or near the highest contour, in the local neighborhood of the peak alone. Instead this optimum direction is derived by giving due weight to the dipole components at far off points in the sky as well, and an optimum direction for the dipole is obtained by minimizing the  $\chi^2$  by fitting  $\cos\psi$  through our COSFIT routine to the dipole amplitudes of all points on the sky.

In Fig. 8 we have shown a contour map of dipole components in different sky directions, determined for the TGSS data for the  $S \geq 100$  mJy sub-sample (Singal 2019a). The best-fit pole position for the TGSS sample, derived from a minimum of the reduced Chi-squared value ( $\chi^2_\nu \lesssim 1$ ), employing our COSFIT routine, is at  $\sim 1\sigma$  of the CMB pole position. Also shown is another independent determination of the dipole from the TGSS data (Bengaly et al. 2018). The dipole from TGSS data seems to lie within a contour of rather high amplitude,  $p \gtrsim 10$ , consistent with earlier determinations (Bengaly et al. 2018; Singal 2019a).

It has been pointed out categorically that the rather high amplitude of dipole in the TGSS data could be a result of calibration problems (Secrest et al. 2022). Incidentally, the pole of the TGSS data turning out to be so close to CMB dipole (Fig. 8), in spite of the calibration errors, if any, cannot be just fortuitous and argues for the TGSS dipole to be reasonably a genuine one. Only in a rather contrived scenario would one expect such a thing to have occurred otherwise. In fact, during a comparison of the flux-density distributions among common sources in the NVSS and TGSS, any mismatches were attributed by Secrest et al. (2022) to calibration errors in the TGSS data alone, which may or may not be fully justified. By applying calibration corrections, the number density of sources in the TGSS sample were apparently adjusted by Secrest et al. (2022) to match those of NVSS data, no wonder the dipole amplitude of the ‘corrected’ TGSS sample turned out to be similar as of the NVSS dipole. Further, thus estimated calibration errors as a function of sky positions by Secrest et al. (2022), when transformed from galactic to equatorial coordinates, can be seen, at least to a first order, to be mainly declination dependent. Now the pole of the TGSS dipole turns out to be almost at the equator, with the antipole direction  $180^\circ$  away, again on or very near the equator (Fig. 8). In such a case any declination-dependent calibration errors will affect the number counts in hemispheres centred on the pole and the antipole almost in the same way and thus not influence the amplitude of the dipole adversely. Whatever else might be the reason for the high amplitude of the TGSS dipole, it does not seem that the sort of calibration errors, as

have been pointed out by Secrest et al. (2022), could mainly be the reason for it.

Similar apparent anomalies in dipole amplitudes have been seen in sources selected from other than the radio surveys as well. For instance, the AGNs picked from the Wide-field Infrared Survey Explorer (WISE) catalogue (Wright et al. 2010; Mainzer et al. 2014) too have yielded dipoles much larger than the CMB dipole (Singal 2021; Secrest et al. 2022). A redshift dipole along the CMB dipole direction in a homogeneously selected DR12Q sample of quasars was seen which, interpreted in terms of the solar peculiar motion, gave a velocity  $\sim 6.5$  times the CMB dipole in a direction directly opposite to, but nonetheless parallel to, the CMB dipole (Singal 2019b). Also a peculiar motion of the observer can introduce a dipole in the  $m - z$  Hubble plot by affecting the observed redshifts ( $z$ ) as well as magnitudes ( $m$ ) of the sources adversely in two opposite hemispheres. This has been exploited to estimate peculiar velocities from the Hubble diagrams of Supernovae (SNe) Ia and of quasars with spectroscopic redshifts (Singal 2022a,b).

An assertion has been made (Dalang & Bonvin 2022) that the differences in dipole amplitudes from the CMB dipole is due to a problem in Eq. (1), where luminosity evolution of the AGN population has not been taken into account. In fact, it has been claimed that if effect of such redshift-dependent luminosity evolution of AGNs on the spectral index  $\alpha$  as well as on the index  $x$  in the integrated source counts is taken into account and one uses thus derived effective  $\alpha$  and  $x$  values in Eq. (1) to derive the peculiar velocity, one gets results consistent with the CMB dipole, in accordance with the CP (Guandalini et al. 2022). Here, however, one has to be careful as the relevant values of  $\alpha$  and  $x$  to be used in Eq. (1), where  $\mathcal{D}$  is estimated from number counts, are not those derived for the whole AGN population, but the values at the threshold flux density of the sample being used. To understand that, one needs to consider the genesis of the dipole asymmetry in number counts due to a peculiar motion of the observer.

As per CP, in the absence of a peculiar motion, the number counts in a sample above an *observed* flux-density threshold, say  $S_0$ , will be the same, apart from the statistical fluctuations, in all directions, irrespective of any redshift distribution or luminosity evolution of the AGN population. However, due to a peculiar motion of the observer, as a result of Doppler boosting, the rest-frame flux-density threshold will be  $S_0/\delta^{1+\alpha}$ . Since the integral source counts of the extragalactic source population follow a power law,  $N(>S) \propto S^{-x}$  (see, e.g., Fig. 1), the number of sources observed at  $S_0$  will be those at  $S_0/\delta^{1+\alpha}$  in the rest frame, which will be higher by a factor  $\delta^{x(1+\alpha)}$ , where both  $\alpha$  and  $x$  are the values in the vicinity of sample flux-density threshold  $S_0$ . Thus the observed number counts will show a dipole asymmetry because sources will move into the sample (or out of it for the opposite hemisphere) by a factor  $\delta^{x(1+\alpha)} \approx 1+x(1+\alpha)(v/c) \cos\theta$ , which has a dipole term ( $\propto \cos\theta$ ), and for the CMB dipole with  $v/c = 1.23 \times 10^{-3}$ , it changes the flux density threshold by a small factor  $1.0022 \cos\theta$  for  $x \approx 1$  and  $\alpha \approx 0.8$ . The relevant values of  $x$  and  $\alpha$  are determined empirically from the actual observations in the vicinity of observed threshold flux density  $S_0$  (Singal 2019a; Tiwari 2019) and with statistical uncertainties  $\lesssim 15\%$ , it will affect the derived peculiar velocity from Eq. (1) to be well within  $\lesssim 10\%$ . Certainly, these will not bring the peculiar motion  $p \sim 4$  close to  $p \sim 1$ , re-

Table 4.

Peculiar velocity,  $\mathbf{v}$ , of the solar system derived from various datasets using different techniques.

(1) Dataset	(2) Waveband	(3) Technique Employed	(4) RA ( $^{\circ}$ )	(5) Dec ( $^{\circ}$ )	(6) $v$ ( $10^3$ km s $^{-1}$ )	(7) Reference
CMB	Microwave	CMB temperature dipole	168	-7	0.37	Aghanim et al. (2020)
NVSS	Radio (1.4 GHz)	Dipole in sky brightness	$153 \pm 9$	$1 \pm 8$	$1.6 \pm 0.4$	Singal (2011)
TGSS	Radio (150 MHz)	Source count dipole	$162 \pm 9$	$3 \pm 8$	$3.8 \pm 0.3$	Singal (2019a)
DR12Q	Optical	Quasar redshift dipole	$166 \pm 10$	$-12 \pm 15$	$-2.4 \pm 0.3$	Singal (2019b)
MIRAGN	Mid IR	Source count dipole	$148 \pm 19$	$23 \pm 17$	$1.7 \pm 0.2$	Singal (2021)
QSOs	Mid IR	Hubble plot dipole	$179 \pm 25$	$42 \pm 25$	$8.1 \pm 1.9$	Singal (2022a)
SNe Ia	Optical	Hubble plot dipole	$173 \pm 12$	$10 \pm 9$	$1.6 \pm 0.5$	Singal (2022b)
WISE	Mid IR	Source density dipole	$142 \pm 6$	$-5 \pm 6$	$0.8 \pm 0.1$	Secrest et al. (2022)
VLASS	Radio (3 GHz)	Source count dipole	$189 \pm 12$	$42 \pm 22$	$1.6 \pm 0.3$	present work
RACS	Radio (887.5 MHz)	Source count dipole	$197 \pm 13$	$-43 \pm 23$	$2.7 \pm 0.3$	present work

quired for the CP to hold good, as claimed in Guandalin et al. (2022). Of course, due to the aberration of light, there is another factor  $\propto \delta^2$  in the observed number densities, which enters Eq. (1), but that, in any case being independent of  $\alpha$  or  $x$ , is not the point of contention here.

The results for various dipoles are summarized in Table 4, which is organized in the following manner: (1) Dataset used. (2) Waveband of observations. (3) Technique employed to compute the dipole. (4) Estimated RA( $^{\circ}$ ) of the corresponding dipole. (5) Estimated Dec( $^{\circ}$ ) of the corresponding dipole. (6) Inferred peculiar velocity,  $v$ , in units of  $10^3$  km s $^{-1}$ . (7) Reference to entries in columns (1) to (6). From Table 4, we see that the peculiar velocity, derived from different datasets, using different techniques, varies by almost an order of magnitude. Combined together, there seems to be an almost overwhelming evidence that the peculiar velocity of the Solar system estimated from the distant radio source distributions in sky is not in concordance with what inferred from the CMB dipole anisotropy.

The sky positions of the poles determined from the VLASS and RACS samples, indicated by  $V$  and  $R$  respectively, are shown along with the error ellipses in Fig. 9. Also shown are the pole positions for other dipoles, along with their error ellipses:  $N$  (NVSS, Singal 2011),  $T$  (TGSS, Singal 2019a),  $Z$  (DR12Q, Singal 2019b),  $M$  (MIRAGN, Singal 2021),  $H$  (Hubble plot of quasars, Singal 2022a),  $S$  (SNe Ia, Singal 2022b) and  $W$  (WISE, Secrest et al. 2022). We have also plotted the “dark flow” dipole, indicated by  $D$ , which is a statistically significant dipole found at the position of galaxy clusters in filtered maps of the CMB temperature anisotropies (Kashlinsky et al. 2010). The CMB pole, at RA=168 $^{\circ}$ , Dec=−7 $^{\circ}$ , indicated by  $\odot$ , has negligible errors (Lineweaver et al. 1996; Hinshaw et al. 2009; Aghanim et al. 2020).

The observed fact that these discordant dipoles, resulting from many independent surveys carried out in different wavebands, are pointing along a narrow band in sky, indicates that these dipoles are somehow related and the cause of the dipoles may be common, otherwise they could have been pointing in random directions in sky. However, not even a single determination of the peculiar velocity from any survey data has yielded a value that may be considered as close to 370 km s $^{-1}$ , determined from CMB dipole asymmetry. The lowest

value for the dipole is at least twice the CMB value, and is obtained from the WISE data (Secrest et al. 2022), although a more recent Bayesian analysis of the number count dipole from the same data has yielded a value about 2.7 times the CMB dipole (Dam, Lewis & Brewer 2022). Almost all other dipoles are much larger in amplitude, with  $p \approx 4$ , corresponding to  $v \approx 1600$  km s $^{-1}$ , being the most common value. Their amplitudes, thus, are not only much larger than the CMB dipole, there is also a statistically significant disparity among themselves in their amplitudes, which does not support a peculiar motion of the Solar system to be that common cause, including that for the CMB dipole. From various dipoles we cannot arrive at a single coherent picture of the solar peculiar velocity, which, defined as a motion relative to the local comoving coordinates, and from the CP a motion with respect to an average universe, should not depend upon the exact data or technique employed for its determination. Therefore such large discrepancies in the inferred velocity vectors may perhaps be a pointer to the need for some rethinking on the conventional interpretation of these dipoles.

Could these dipoles, which exhibit some excess of source densities in certain sky directions, be due to some unaccounted for random fluctuations or some not understood systematics in the data or the technique? Now in such a scenario the dipoles should be pointing in random directions in sky. However, there are at least 9 statistically independent determinations of dipoles, counting MIRAGN and WISE samples as one point as they have partial overlap of data and thus may not be treated as completely independent data points. All of these nine points seem to point in a narrow sky region ( $\lesssim 1/6$ th of the total) about the CMB dipole, which, by a conservative estimate, has a probability  $\lesssim (1/6)^9 \approx 10^{-7}$ , to occur by a random chance.

One has to explain the pointing of all these dipoles in a narrow region of sky and what is so special about this direction in sky and whether it represents some sort of an “axis” of the universe. Further, various dipole magnitudes differing by as much as an order of magnitude, if interpreted as due to our peculiar velocity with respect to them, indicates that there may be a large relative motion of the various cosmic reference frames. Significant differences in their derived peculiar velocities may be indicating that different cosmic reference frames

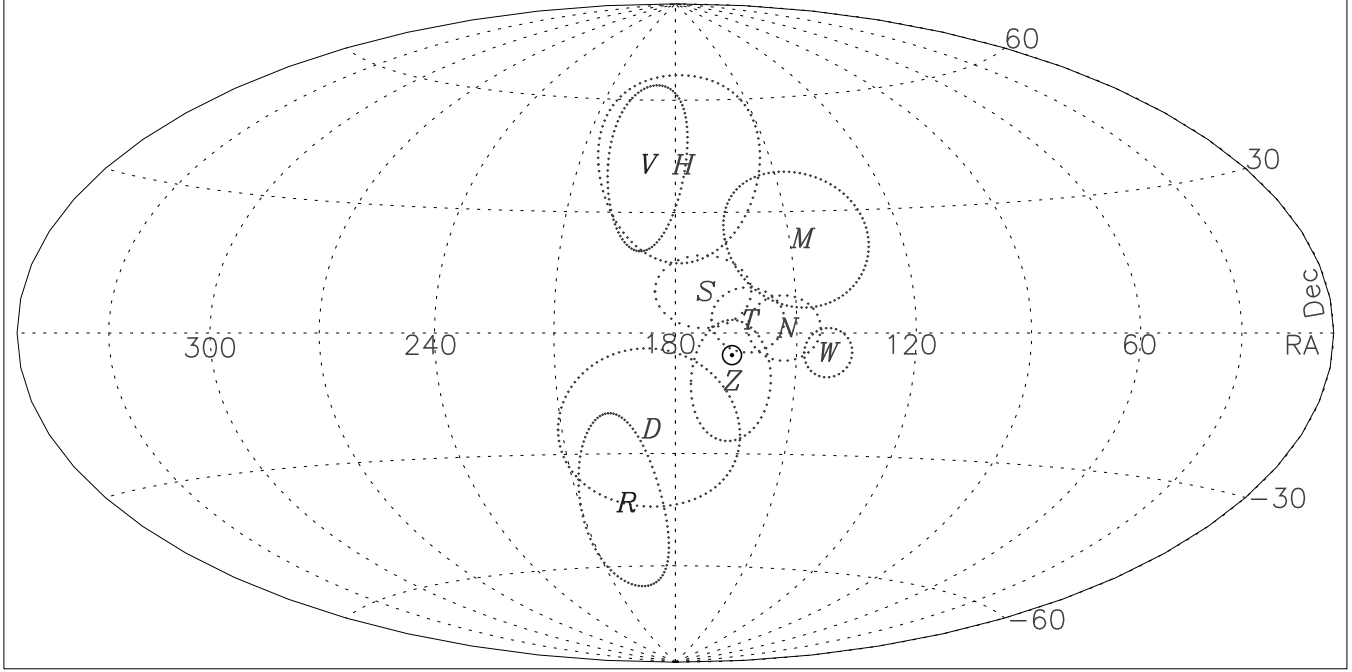


**Figure 9.** The sky, in the Hammer–Aitoff equal-area projection, plotted in equatorial coordinates RA and Dec, showing the positions of the poles determined from the VLASS and RACS samples, indicated by  $V$  and  $R$  respectively, along with their error ellipses at  $1\sigma$  (68.3%) confidence limits. Also shown on the map are the other pole positions for various dipoles along with their error ellipses,  $N$  (NVSS),  $T$  (TGSS),  $Z$  (DR12Q),  $M$  (MIRAGN),  $H$  (Hubble plot of quasars),  $S$  (SNe Ia),  $W$  (WISE) and  $D$  (Dark Flow). The CMB pole, at  $\text{RA} = 168^\circ$ ,  $\text{Dec} = -7^\circ$ , indicated by  $\odot$ , has negligible errors.

are moving relative to each other or that the matter distribution on cosmic scales is not homogeneous and isotropic, in contravention of what expected from the CP, which is the starting point for the standard modern cosmology. There is other corroborating evidence that puts doubt on concurrency of the observable Universe with the CP (Aluri et al. 2023). Perhaps there is need for a fresh look at the role of the CP in the cosmological models.

## 5 CONCLUSIONS

From the dipole anisotropies seen in the sky distribution of sources in the VLASS and RACS surveys, the inferred peculiar motion of the Solar system turns out a factor of four to seven higher than what inferred from the CMB dipole. The directions of radio dipoles in the two datasets differ significantly not only from the CMB dipole but also from each other. However these as well as other previously determined cosmic dipoles seem to point toward a relatively narrow region of the sky, which crudely speaking, has a low probability, less than one part in  $10^7$ , by a random chance. This indicates a preference for certain sky direction for these dipoles, which seems discordant with the cosmological principle, the basis of modern cosmology.

## DATA AVAILABILITY

The VLASS data used in this article are available in VizieR Astronomical Server in the public domain at <http://vizier.u-strasbg.fr/viz-bin/VizieR>. The dataset is downloadable by

selecting catalog: J/ApJS/255/30/comp. Another, independent version of the VLASS catalogue can be found in the electronic edition of the Astrophysical Journal in FITS format at <https://iopscience.iop.org/article/10.3847/1538-4357/abf73b/meta>. The RACS catalogue is available at <https://doi.org/10.25919/8zyw-5w85> under Files as the file RACS\_DR1\_Sources\_GalacticCut\_v2021\_08.xml.

## DECLARATIONS

The author has no conflicts of interest/competing interests to declare that are relevant to the content of this article. No funds, grants, or other support of any kind was received from anywhere for this research.

## REFERENCES

- Aghanim N. et al., 2020, A&A, 641, A1
- Aluri P. K. et al., 2023, Class. Quant. Grav., 40, 094001
- Baleisis A., Lahav O., Loan A. J., Wall J. V., 1998, MNRAS, 297, 545
- Bengaly C. A. P., Maartens R., Santos M. G., 2018, J. Cosm. Astropart. Phys., 4, 31
- Bevington P. R., Robinson D. K., 2003, Data reduction and error analysis for physical sciences. 3rd edn. McGraw, New York
- Blake C., Wall J., 2002, Nature, 416, 150
- Bruzewski S., Schinzel F. K., Taylor G. B., Petrov L., 2021, APJ, 914, 42
- Colin J., Mohayaee R., Rameez M., Sarkar S., 2017, MNRAS, 471, 1045
- Condon J. J., Cotton W. D., Greisen E. W., Yin Q. F., Perley R. A., Taylor G. B., Broderick J. J., 1998, AJ, 115, 1693

Crawford F., 2009, *ApJ*, 692, 887  
 Dalang C., Bonvin, C., 2022, *MNRAS*, 512, 3895  
 Dam L., Lewis G. F., Brewer B. J., 2022, ArXiv:2212.07733  
 Darling, J., 2022, *ApJ*, 931, L14  
 Ellis G. F. R., Baldwin J. E., 1984, *MNRAS*, 206, 377  
 Gordon Y. A. et al., 2021 *ApJS*, 255, 30  
 Guandalin C., Piat J., Clarkson C., Maartens R., 2022, ArXiv:2212.04925  
 Hale C. L. et al. 2021, *Publ. Astron. Soc. Australia* 38, e508  
 Hinshaw G. et al., 2009, *ApJS*, 180, 225  
 Intema H. T., Jagannathan P., Mooley K. P., Frail D. A., 2017, *A&A*, 598, A78,  
 Kashlinsky, A., Atrio-Barandela, F., Ebeling, H., Edge, A., Kovcevski, D., 2010, *ApJ*, 712, L81  
 Lacy M. et al., 2020, *PASP*, 132, 035001  
 Lineweaver C. H., Tenorio L., Smoot G. F., Keegstra P., Banday A. J., Lubin P., 1996, *ApJ*, 470, 38  
 Mainzer A. et al., 2014, *ApJ*, 792, 30  
 Rubart M., Schwarz D. J., 2013, *A&A*, 555, A117  
 Secret N. J., Hausegger S. V., Rameez M., Mohayaee R., Sarkar S., Colin J., 2021, *ApJ*, 908, L51  
 Secret N., Hausegger S. V., Rameez M., Mohayaee R., Sarkar S., 2022, *ApJ*, 937  
 Siewert T. M., Rubart M. S., Schwarz D. J., 2021, *A&A*, 653, A9  
 Singal A. K., 2011, *ApJ*, 742, L23  
 Singal A. K., A. K. 2014, *A&A*, 568, A63  
 Singal A. K., 2019a, *Phys. Rev. D*, 100, 063501  
 Singal A. K., 2019b, *MNRAS*, 488, L104  
 Singal A. K., 2021, *Universe* 7, 107  
 Singal A. K., 2022a, *MNRAS*, 511, 1819  
 Singal A. K., 2022b, *MNRAS*, 515, 5969  
 Swarup G., Ananthakrishnan S., Kapahi V. K., Rao A. P., Subrahmanyam C. R., Kulkarni V. K. 1991, *Current Science*, 60, 95  
 Tiwari P., 2019, *Res. Astr. Astrophys.*, 19, 96  
 Tiwari P., Kothari R., Naskar A., Nadkarni-Ghosh S., Jain P., 2015, *Astropart. Phys.*, 61, 1  
 Wright E. L. et al., 2010, *AJ*, 140, 1868